Supporting information for:

Trimethyltin Mediated Covalent Gold-Carbon Bond Formation

Arunabh Batra,[†] Gregor Kladnik,[‡,¶] Narjes Gorjizadeh,[§,‖] Jeffrey Meisner,[⊥] Michael Steigerwald,[⊥] Colin Nuckolls,[⊥] Su Ying Quek,[*,§,‖] Dean Cvetko,[¶] Alberto Morgante,[*,¶,#] and Latha Venkataraman[*,†]

Department of Applied Physics and Applied Mathematics, Columbia University, New York, NY, Department of Physics, University of Ljubljana, Ljubljana, Slovenia, CNR-IOM Laboratorio Nazionale TASC, Basovizza SS-14, km 163.5, I-34012 Trieste, Italy, Department of Physics, National University of Singapore, Singapore, Institute of High Performance Computing, Agency for Science, Technology and Research, Singapore, Department of Chemistry, Columbia University, New York, NY, and Department of Physics,University of Trieste, Trieste, Italy

E-mail: phyqsy@nus.edu.sg; morgante@iom.cnr.it; lv2117@columbia.edu

[*]To whom correspondence should be addressed
[†]Department of Applied Physics and Applied Mathematics, Columbia University, New York, NY
[‡]Department of Physics, University of Ljubljana, Ljubljana, Slovenia
[¶]CNR-IOM Laboratorio Nazionale TASC, Basovizza SS-14, km 163.5, I-34012 Trieste, Italy
[§]Department of Physics, National University of Singapore, Singapore
[‖]Institute of High Performance Computing, Agency for Science, Technology and Research, Singapore
[⊥]Department of Chemistry, Columbia University, New York, NY
[#]Department of Physics,University of Trieste, Trieste, Italy

Experimental Methods

Sample Preparation

The Au substrates are first cleaned by repeated cycles of Ar sputtering and annealing to 800K. Reflection high-energy electron diffraction (RHEED) is then used to confirm the characteristic 1x2 missing-row reconstruction of the Au(110) substrate. XPS measurements of the Au are made to ensure no contamination on the sample. The operational pressure for the measurement chamber is maintained at 10^{-10} mbar. Benzyltrimethylstannane (synthesized following published procedures[S1]) is deposited on this substrate through a leak valve at a chamber pressure of 10^{-7} mbar.

X-ray Photoemission Spectroscopy Measurements

X-ray photoemission spectroscopy (XPS) measurements were performed at the ALOISA beamline[S2] with the x-ray beam at grazing-incidence (4^o) to the sample and with the electric field perpendicular to the sample (p-pol). The photon energy of 650 eV was used for XPS with an overall energy resolution (photon + electron analyzer) of $\sim$ 200 meV. Photoelectrons from the sample were collected normal to the surface using a hemispherical electron analyzer with an acceptance angle of 2^o, and overall energy resolution of $\sim$ 0.2 eV. The energy scale for XPS spectra was calibrated by aligning the Au $4f_{7/2}$ peak to a binding energy of 84.0 eV, or where identified, aligning the Fermi energy to zero.

Near Edge X-Ray Absorption Fine Structure

Near Edge X-Ray Absorption Fine Structure (NEXAFS) measurements were conducted on the carbon K-edge, with incident photon energy varied in steps of 0.1 eV between 280 eV and 310 eV. The photon incidence angle was set to 6^o. Spectra were acquired using a channeltron detector with a wide acceptance angle in partial electron yield mode, with a high pass filter set to 250 eV. The photon flux was monitored on the last optical element along the beam

path and a separate measurement of NEXAFS signal was taken on a clean Au substrate for normalization. The sample normal was oriented either parallel to the photon polarization (p-pol) or perpendicular to polarization (s-pol). These measurements were used to determine the orientation of the molecules on the surface (NEXAFS linear dichroism measurement) as follows. The relative intensity of the NEXAFS signal in s-pol and p-pol for the C1s $\rightarrow$ π^*-LUMO transition is used to obtain the orientation of the aromatic ring relative to the surface. The angle θ of the ring to the surface is determined as $\theta = \tan^{-1}\sqrt{2I_s/I_p}$ where I_s and I_p are the intensities of the LUMO NEXAFS peak from the s-pol and p-pol spectra.

Calculation of Stoichimetric ratios from XPS

The expected XPS signal ratio for carbon to tin is given by:

$$\frac{I_{expected,C1s}}{I_{expected,Sn3d}} = \frac{\sigma_{C1s} \cdot N_C \cdot \int_0^d \exp(\frac{-x}{\lambda_{C1s}})dx}{\sigma_{Sn3d} \cdot N_{Sn} \cdot \int_0^d \exp(\frac{-x}{\lambda_{Sn3d}})dx}$$

where σ is the interaction cross section for incident X-rays at 650 eV, N is the number of atoms in a molecule, $I_{expected}$ is the expected XPS intensity calculated by taking the area under the XPS peak, d is the thickness of the film, and λ is the inelastic mean free path (IMFP) of outgoing electron signal (kinetic energy dependent) due to inelastic scattering with surrounding (and overlayer) molecules. Cross section data is obtained from Yeh and Lindau.[S3] The IMFP is calculated using the standard formula as discussed in Cumpson and Seah.[S4] A calculated density of 1.327 g/cm^3 is used for trimethylbenzylstannane.

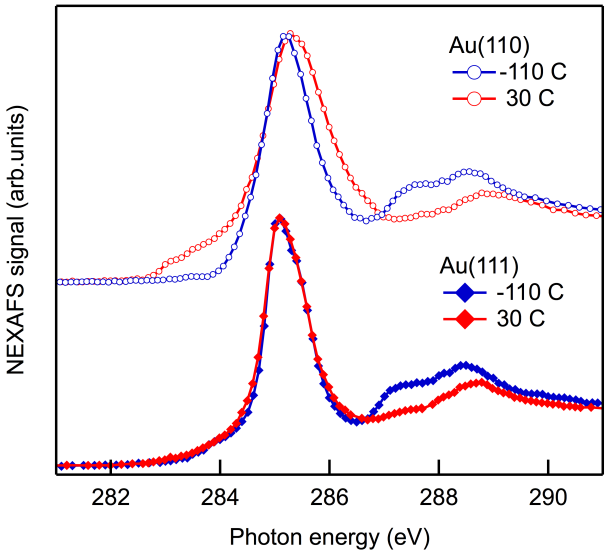

Figure S1: NEXAFS spectra of benzyltrimethylstannane on Au(110) and Au(111) measured in p-pol geometry. All spectra have been normalized by the photon flux measured separately on clean Au substrates. Substantial broadening ($\sim$ 1eV) of the dominant π^* peak at 285 eV is seen for benzyltrimethylstannane/Au(110) upon heating to 30 C, which correlates with the occurrence of the gap state at 283.5 eV. No π^* peak broadening nor gap state formation is observed for benzyltrimethylstannane/Au(111).

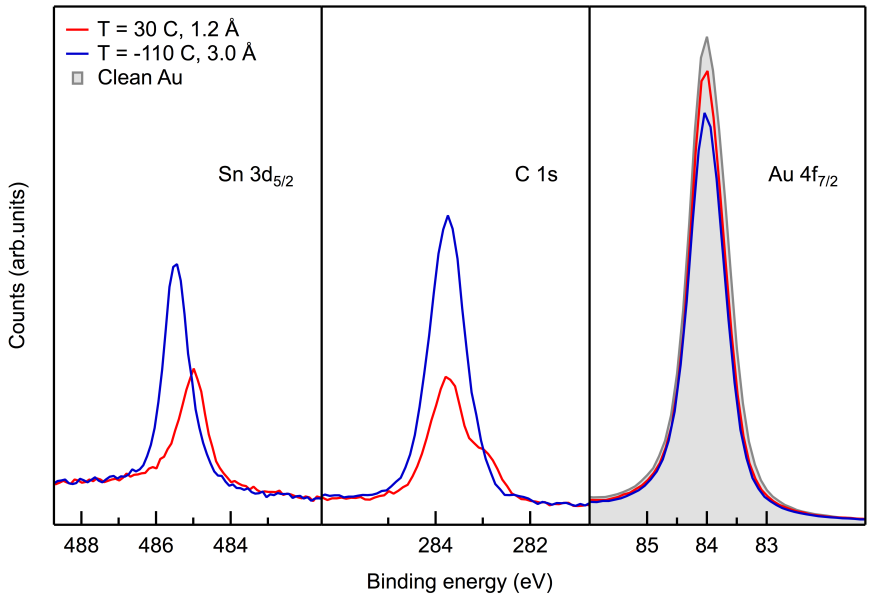

Figure S2: XPS of Au $4f_{7/2}$ C1s and Sn $3d_{5/2}$ with 650 eV photon energy. From the attenuation of the Au 4f intensity an equivalent benzyltrimethylstannane layer thickness of 3.0 and 1.2 is obtained for T= -110 C and T= + 30 C, respectively.

Theoretical Methods

Reaction Pathway Calculations

To find the preferred binding sites of the cleaved fragments on Au, we relax benzyl and trimethyltin on the Au(111)+adatom using the plane-wave pseudopotential method as implemented in the VASP 5.2 code[S5] with projector-augmented-wave pseudopotentials.[S6] The van der Waals density functional method with optB86b functional is included for calculating the non-local vdW interactions between the molecule and the surface. The vdW_optB86b functional predicts the lattice constant of Au 1% smaller than the experimental value (4.08 Å), which is the closest value compared to other functionals, such as vdW_revPBE, vdW_optB88 and vdW-DF2, in agreement with Klimes, Bowler and Michaelides.[S7] Using this vdW functional, the relaxed intact molecule on Au(111) has a tilt angle of 83^o between the plane of the phenyl ring and the surface normal, in excellent agreement with experiment.

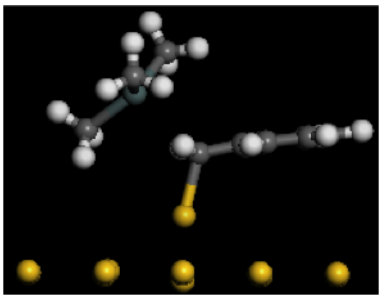

Figure S3: Transition state for dissociation of molecule on Au adatom obtained from constrained relaxation technique. The transition state obtained from constrained relaxation is similar to the one obtained from NEB calculation shown in Figure 4 of the manuscript.

Benzyl and trimethyltin are relaxed on Au(111) flat surface on atop, bridge, hollow FCC and hollow HCP sites, and also on adatom on Au (111) surface. Six layers of Au with a 4x4 supercell (16 atoms per layer) are considered, where the three bottom layers are fixed and the rest are allowed to relax. A Monkhorst-Pack 2x2x1 k-point mesh is used for the relaxations and a 4x4x1 mesh is used to calculate the total energies. The cut-off energy for the plane-wave expansion is set to 400 eV. Calculation of binding energies of benzyl and trimethyltin on Au on different binding sites shows that trimethyltin strongly favors binding

to the flat Au(111) surface, being ∼0.4 eV more stable on Au(111) than on the Au adatom (the different binding sites on flat surface have very similar binding energies; see Table S1. On the other hand, the binding energy for benzyl on the Au adatom is only ∼0.1 eV less stable than on the favored (atop) binding site on Au(111). These results indicate that there is a larger probability for benzyl to bind to adatom sites compared to trimethyltin.

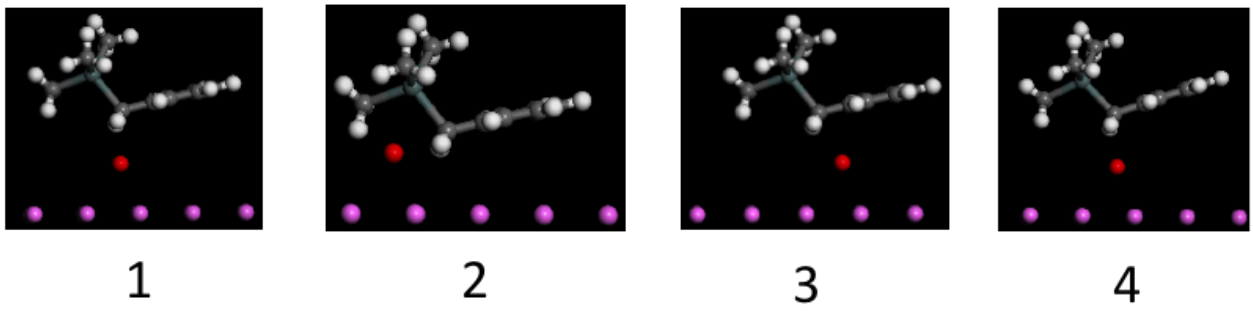

Figure S4: Relaxed structures of intact molecule on Au adatom on Au(111) with different positions relative to adatom. Structure 1 is the most favorable structure.

Table S1: Binding energies (eV) (E_b=$E_{Au+molecule}$-E_{Au}-$E_{molecule}$) of benzyl and $SnMe_3$ on Au on different binding sites using vdW-optB86b functional. Total energy of molecule fragment is obtained by spin-polarized calculations.

Molecular Fragment	**Au adatom //Au(111)**	**Au(111)-atop**	**Au(111)-bridge**	**Au(111)-hollowFCC**	**Au(111)-hollow HCP**
$SnMe_3$	-2.18	-2.60	-2.61	-2.59	-2.63
Benzyl	-1.75	-1.87	-1.74	-1.13	-1.22

Table S2: Binding energies (eV) (E_b=$E_{Au+molecule}$-E_{Au}-$E_{molecule}$) of benzyl and $SnMe_3$ on Au on different binding sites using PBE functional without van der Waals energies. Total energy of molecule fragment is obtained by spin-polarized calculations.

Molecular Fragment	**Au adatom //Au(111)**	**Au(111)-atop**	**Au(111)-bridge**	**Au(111)-hollowFCC**	**Au(111)-hollow HCP**
$SnMe_3$	-1.85	-1.70	-1.66	-1.62	-1.67
Benzyl	-1.29	-0.51	-0.59	-0.58	-0.52

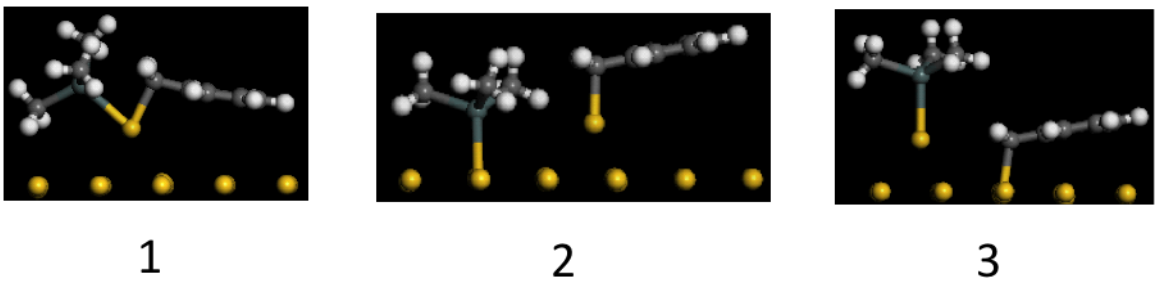

Figure S5: Final configurations of benzyl and $SnMe_3$ bound to different sites (adatom on Au surface). Structures 1-2 are more stable than structure 3 by ∼0.6 eV. Structure 1 is the most favorable, being ∼0.04 eV more stable than structure 2.

To compute the minimum energy path (MEP) for the dissociation of the intact molecule on flat Au(111) and Au(111) with Au adatoms, we used a larger 6x6 supercell and included 4 fully-relaxed Au layers in the calculations. We have checked that the relative binding energies for the molecular fragments are essentially the same when using 4 fully-relaxed Au layers instead of 6 Au layers. For the MEP with Au adatoms, we used the climbing-image nudged elastic band (CI-NEB) method as implemented in VASP.[S5] This CI-NEB method guarantees that the maximum energy in the MEP is a saddle point in the energy surface.

NEXAFS Calculations

Molecules were structurally relaxed by performing spin-unrestricted calculations using the B3LYP exchange-correlation functional and LACVP basis set using the Q-Chem software suite.[S8] Default grids and convergence thresholds were used for relaxation. Subsequently, single-point calculations were carried out using B3LYP/LACVP* to calculate molecular energy levels. For NEXAFS simulations and orbital isosurfaces of Carbon K-edge excited molecules, GPAW, a grid-based real-space projector-augmented-wave code was employed with the B3LYP exchange-correlation functional.[S9] Isolated molecules were first relaxed to their optimized geometries, before conducting single point calculations. Default grid spacings and convergence thresholds were employed. All NEXAFS calculations were performed using the half-core-hole approximation.[S10]

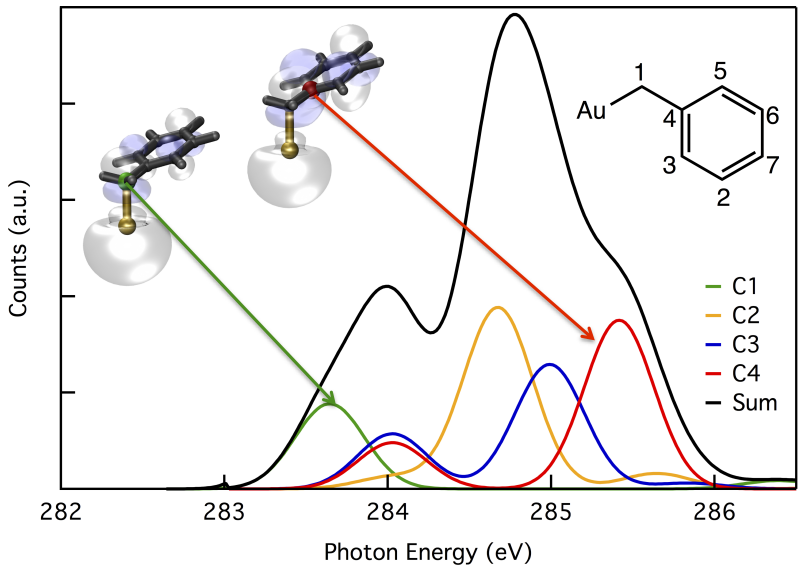

Figure S6: Calculated NEXAFS spectra for Au_1-Benzyl. Colored curves correspond to simulated NEXAFS spectra with a core hole on corresponding carbon atom. Black curve is the total NEXAFS spectrum. The main peak at 285 eV corresponds to excitation on carbon atoms on the benzene ring (excluding C1). The peak centered at 284 eV is a result of excitations on the benzyl carbon (C1, green) or its nearest carbon neighbor (C4, red).

References

(S1) Chen, W.; Widawsky, J. R.; Vazquez, H.; Schneebeli, S. T.; Hybertsen, M. S.; Breslow, R.; Venkataraman, L. *Journal of the American Chemical Society* **2011**, *133*, 17160–17163.

(S2) Floreano, L.; Naletto, G.; Cvetko, D.; Gotter, R.; Malvezzi, M.; Marassi, L.; Morgante, A.; Santaniello, A.; Verdini, A.; Tommasini, F.; Tondello, G. *Review of Scientific Instruments* **1999**, *70*, 3855–3864.

(S3) Yeh, J. J.; Lindau, I. *Atomic Data and Nuclear Data Tables* **1985**, *32*, 1–155.

(S4) Cumpson, P. J.; Seah, M. P. *Surface and Interface Analysis* **1997**, *25*, 430–446.

(S5) Kresse, G.; Furthmuller, J. *Physical Review B* **1996**, *54*, 11169–11186.

(S6) Blochl, P. E. *Physical Review B* **1994**, *50*, 17953–17979.

(S7) Klimes, J.; Bowler, D. R.; Michaelides, A. *Journal of Physics-Condensed Matter* **2010**, *22*.

(S8) Shao, Y.; Molnar, L. F.; Jung, Y.; Kussmann, J.; Ochsenfeld, C.; Brown, S. T.; Gilbert, A. T. B.; Slipchenko, L. V.; Levchenko, S. V.; O'Neill, D. P.; DiStasio Jr, R. A.; Lochan, R. C.; Wang, T.; Beran, G. J. O.; Besley, N. A.; Herbert, J. M.; Yeh Lin, C.; Van Voorhis, T.; Hung Chien, S.; Sodt, A.; Steele, R. P.; Rassolov, V. A.; Maslen, P. E.; Korambath, P. P.; Adamson, R. D.; Austin, B.; Baker, J.; Byrd, E. F. C.; Dachsel, H.; Doerksen, R. J.; Dreuw, A.; Dunietz, B. D.; Dutoi, A. D.; Furlani, T. R.; Gwaltney, S. R.; Heyden, A.; Hirata, S.; Hsu, C.-P.; Kedziora, G.; Khalliulin, R. Z.; Klunzinger, P.; Lee, A. M.; Lee, M. S.; Liang, W.; Lotan, I.; Nair, N.; Peters, B.; Proynov, E. I.; Pieniazek, P. A.; Min Rhee, Y.; Ritchie, J.; Rosta, E.; David Sherrill, C.; Simmonett, A. C.; Subotnik, J. E.; Lee Woodcock Iii, H.; Zhang, W.; Bell, A. T.; Chakraborty, A. K.; Chipman, D. M.; Keil, F. J.; Warshel, A.; Hehre, W. J.; Schaefer Iii, H. F.; Kong, J.; Krylov, A. I.; Gill, P. M. W.; Head-Gordon, M. *Physical Chemistry Chemical Physics* **2006**, *8*.

(S9) Mortensen, J. J.; Hansen, L. B.; Jacobsen, K. W. *Physical Review B* **2005**, *71*, 035109.

(S10) Nilsson, A.; Pettersson, L. G. M. *Surface Science Reports* **2004**, *55*, 49–167.